# *Demystifying the Dynamics of Global and Regional Sea Level Trends from 1993 to 2021*

Ashraf Rateb[1]; Bridget R. Scanlon[1]

[1]Bureau of Economic Geology, University of Texas at Austin, Austin 78758, Texas United States

Correspondence to (ashraf.rateb@beg.utexas.edu)

## Abstract

As global sea levels rise, questions persist about the robustness of trends and their dynamics. Here, we offer a fresh perspective by examining the dynamics of global and regional mean sea-level trends using a probabilistic framework applied to the altimetric record. We show that the global mean sea-level (GMSL) rise accelerated from 2.5 mm/yr (1993-2000) to 4.2 mm/yr (2014-2021) with an average plausibility (85%) over the entire 29-year record. El-Niño Southern Oscillation modulates GMSL, with ~9% increase (decrease) in magnitude during El-Niño (La-Niña) events. Furthermore, our analysis identifies six regions (e.g., Pacific, Atlantic, Indian, Tropics, Southern Oceans and North Sea) with high probability of upward stable trends that persisted beyond interannual and decadal natural variability of arbitrary 29-year window, −suggesting a substantial contribution from external factors (e.g., climate change). By treating sea level trends as random processes and employing non-parametric probabilistic methods (e.g., Gaussian process regression) we obtain reliable estimates that account for trends complex patterns and inherent uncertainties, ultimately enhancing attribution processes and facilitating effective communication of sea level trend changes.

## Introduction

As a vital gauge of climate change, the global mean sea level (GMSL) has consistently risen over the past century [1], with an acceleration observed in recent decades [2,3] based on robust evidence from tide gauge records, satellite altimetry, and climate models[4]. This trend is attributed to various factors, including the thermal expansion of seawater, melting ice sheets and glaciers, and changes in the ocean circulation [5]. Nonetheless, acceleration of the GMSL during the satellite altimetry era (1992 – present) remains a subject of debate and uncertainty. While some studies propose that external forces such as climate change drive the acceleration [2], others maintain that multidecadal natural variability offers an equally plausible explanation [6]

Regarding regional mean sea level (RMSL) trends, there is an ongoing debate about the origins of their changes. It remains uncertain whether these trends are primarily due to natural climate variability in the oceans or if they are influenced by external forces akin to those affecting GMSL. These uncertainties can be attributed to factors such as limitations in data sources, lack of comprehensive knowledge about the interactions between external and internal forces, and constraints presented by conventional methodologies of trend estimations and attributions. The satellite altimetry record, covering only three decades (1992-present), and has already yielded accurate measurements of sea surface height for both GMSL and RMSLs[7]. However, the relatively short duration of the record remains insufficient to fully account for the timescale of the natural climate variability[8]. The methods used to assume sea-level trends and their changes adhere to the traditional assumptions that the trends are deterministic and distinct from random climate variability. Typically, trends are defined as "*long-term variations of statistical properties, such as the mean*"[9]. However, this definition is not directly applicable to sea level trends/changes because of short-term fluctuations (e.g., seasonal and interannual) where natural climate variability, such as the El-Niño Southern Oscillation (ENSO), masks external forcing impact (e.g., greenhouse gas [GHG] concentration rises) [10,11]. Alterations in the mean of regional and coastal sea levels can result from sub-seasonal water level fluctuations originating from distant regions, such as extratropical cyclones[12] or small-scale turbulence. These factors, when combined with atmospheric influences, can contribute to

random sea-level fluctuations over several decades, complicating the long-term attribution of coastal sea-level changes. Therefore, changes in sea-level trends may be better understood as random process[13]. Assessing changes in sea-level trends using various methods and assumptions can yield inconsistent results for GMSL and RMSL, even when considering 100 years of data[14]. Visser, et al. [15] identified 33 modeling options, including parametric deterministic modeling, parametric low-pass filtering, non-parametric smoothing, stochastic modeling, and miscellaneous modeling. The complexities of these methods range from simple regression to advanced filtering techniques. The variability of these statistical methods results in conclusions that can be driven by the models themselves rather than by the data (e.g., debates on the acceleration and deceleration of sea-level rise)[16-19].

Moreover, evaluating the robustness of sea-level trends and identifying changes in trends using traditional deterministic approaches has proven to be analytically challenging. Conventional methods, such as tail-area significance tests, do not fully establish the reliability of trend hypotheses and their interpretation is often arbitrary[20,21]. Kim, et al. [22] proposed a variation of the widely-used Hodrick-Prescott filter, which effectively decomposes time series into trends and cyclical components. This new approach uses absolute values instead of squares, resulting in piecewise linear trend estimates that better capture abrupt changes in the time-series data. Change-point detection methods[23-25] require abrupt changes; however, changes in sea-level trends can be gradual and continuous rather than abrupt. Gottlieb and Müller [26] introduced the stickiness coefficient as a measure of co-variation of trend deviations over time, but this coefficient is difficult to interpret. In summary, traditional deterministic methods for assessing sea-level trends and their changes can be questioned and undermined.

In contrast, Jensen and Ekstrøm [27] proposed two probabilistic indices to quantify the trend strength and changes based on the likelihood and frequency of such changes.

Sea-level trends and related changes can be considered stochastic process for two main reasons. First, the factors influencing sea level trends are partly random in nature (e.g., natural climate variability), and the interactions between these factors and external elements (e.g., climate change) are characterized by significant uncertainty. This makes it challenging to predict changes in these trends[10]. The linear feature of sea-level trends represents a persistent change in these driving factors and reveals the timescale of the driving process. Second, observations of sea-level trends are imperfect because of systematic errors and inherent data uncertainty in the altimeter record, or spatiotemporal subsampling in the tide gauge. Moreover, from a practical perspective assessing trends/changes in trends of sea-level rise as random processes is practical for coastal management, as it clarifies trend variability and addresses uncertainties.

Therefore, utilizing stochastic models based on a probabilistic framework is essential to account for these uncertainties and provide accurate quantification and prediction of sea-level trends and changes. The objective of this study was to address the following three key questions.

  1) How did GMSL and RMSL trends change over the last 29 years (1993 – 2021)?
  2) How does natural climate variability, such as ENSO, modulate the GMSL trends?
  3) Do RMSLs exhibit persistent trends beyond those linked to natural climate variability?

We used latent Gaussian process regression modeling to analyze GMSL and RMSL data and derived trend magnitude and two trend change indices. The Trend Direction Index (TDI) measures the probability of a change in the upward trend from 0 to 100%, whereas the complement (100 – TDI) refers to the probability of a downward trend. A 50% of TDI implies a neutral change and epistemic uncertainty, whereas a TDI of < 50% indicates a downward trend. The mean TDI value over a particular period (e.g., the data length spanning 1993 to 2021) signifies the degree of plausibility associated with the observed trend. Second, the Trend Shift Score (TSS) evaluates the trend stability by counting the number of slope sign changes Lower TSS scores signify stable trends while higher scores suggest instability. Notable TSS changes highlight the influence of driving processes to modulate the trend magnitude, direction, and stability. TSS can also be used to estimate the likelihood of a trend reversal within a specific period. These metrics, combined with the trend magnitude, are valuable for assessing changes in sea-level trends and are applicable to any climate data. Lastly, we use the term "acceleration" to refer to a shift in the

distribution of trend properties, specifically magnitude, TDI, and TSS, meaning the trend became higher in magnitude, more plausible (higher TDI), and more stable (lower TSS). This differs from the conventional definition, which typically refers to the parametric value of quadratic fits.

Using these tools, we assessed the GMSL and RMSL trends and their dynamics based on a 29-year altimetry record. Our findings indicate that GMSL rise has high average plausibility (TDI: 85±9%); with a low probability of trend reversal (15%). GMSL exhibits temporary pauses during La Niña events, with approximately symmetric accelerations occurring during El Niño events. Moreover, GMSL and six RMSL regions, which encompass a significant portion of the world's oceans, display a shift in the distribution of three key parameters: magnitude, TDI, and TSS. The observed trends in these regions tend to demonstrate higher magnitudes, increased TDI, and greater stability (i.e., lower TSS: lower likelihood of reversal). These findings indicate a consistently stable upward trend, extending beyond the oscillations observed within a 29-year arbitrary window (representing the length of the altimetry dataset). All results are presented with a 95% credible interval.

## Results

## Global mean sea-level rise, acceleration, and episodic pauses

The GMSL represents the average surface height of the entire oceans. Over the 29-year (1993-2021), the altimetry data show an upward GMSL trend at a mean rate of 3.1 mm/yr with plausibility of 85±9% and a 15% probability of a trend reversal (Fig 1a). This trend magnitude and plausibility account for all GMSL rises driven by external forcing (e.g., GHG) or internal processes (e.g., natural climate variability, e.g., ENSO etc) and represent the average of various changes (i.e., constant, linear, and quadratic) over the 29-year period. Throughout 1993-2021, the GMSL exhibits varying dynamic properties (Table 1) but consistently increases in magnitude, plausibility, and stability. The average GMSL trend magnitude increased over time from 2.8 mm/yr with a plausibility of 83±7% (1993 – 2013) to 4.2 mm/yr with a plausibility of 90±7% (2014 – 2021) representing an increase in magnitude of 1.4 mm/yr and a 7% increase in plausibility. The GMSL TSS of 0.41 over the entire 29 years has a low probability (1.4%) of a downward trend (e.g., sea-level fall). The observed persistence in trend magnitude, plausibility, and stability signifies a consistent GMSL increase, transcending the fluctuations of interannual and decadal natural variability observed over a 29-year period. It is crucial to note that the 29-year oscillation represents a hypothetical window corresponding to the length of the data record and does not inherently reflect actual natural variability within the ocean system. The persistence of the GMSL trend over this period suggests a significant contribution from external forcing, such as ocean warming and mass balance redistribution from ice sheets, glaciers, and land water storage. Over the 29-yr period from 1993 to 2021, there are pauses in the upward trend in the GMSL at an inter-annual scale. Five periods of slowdown were identified when the TDI fell below 50%: 1998-1999, 2007-2008, 2010-2011, 2013, and 2016-2017. These periods correspond to moderate-to-strong La Niña events in the eastern and central Pacific Oceans (Fig. 1). Although the anomaly in 2013 is not classified as a La Niña period because it did not surpass a -0.5 anomaly (with ONI values ranging from -0.4 to 0.3), it corresponds to a decrease in GMSL trend magnitude of -0.41 mm and a slowdown in the trend as if GMSL is trending with 55% in the downward trend direction (Table 1). The detection of these minor changes highlights the robustness of the regression model and the valuable insights that the TDI provide. The strength and duration of La Niña events appear to impact the TDI and TSS of the upward GMSL trends and increase the probability of trend reversal (i.e., a downward trend). Slowing GMSL trends were also observed during weak La Niña events, such as 2005-2006 and 2020-2022 where the TDI decreased by 25-30% (Fig 1). We assessed the trend properties of GMSL by examining the data on a monthly basis in relation to the ONI status. During the neutral phase, which accounts for 46% of the data spanning 158 months, the average GMSL magnitude is 3.17 mm/yr, with TDI of 88%. In the El Niño phase, which covers only 23% of the data over 78 months, the GMSL magnitude increases to 3.4 mm/yr, while the TDI decreases to 84%. Conversely, during the La Niña phase, which constitutes 30% of the data across 101 months, the GMSL magnitude drops to 2.8 mm/yr, and the TDI declines to 82%. On average, El Niño events accelerate the trend magnitude by 9%, while La Niña events decelerate it. The 4% decrease in TDI during El Niño compared to the neutral phase (88%)

can be attributed to the smaller sample size of El Niño months relative to the neutral phase (as detailed in Tables **S3-S5**).

## Regional Mean Sea Level Rise and Acceleration

From 1993 to 2021, the mean sea level trend across 21 zones was 3.2 mm/yr and accompanied with TDI of 61% ±19% (Fig 2). Notably, 13 of these regions displayed small TDI values ranging from 50% to 59% and higher uncertainties between 10% and 36%, suggesting that the plausibility of upward changes is not consistently reliable over the 29-year period. In contrast, we identified six RMSL hotspots with upward trend plausibility, covering much of the global oceans, including the Pacific, Atlantic, Southern, Tropical, and Indian oceans as well as the North Sea (Fig 3). These hotspots exhibit trend magnitudes ranging from 3.0 to 3.6 mm/yr, plausibility degree ranges from 64% to 100% with uncertainties of 1-19%, and TSS ranges between 0.1% and 5.0% over the 29-year period (Fig. 2). Moreover, the trends in the six regions persist over time, where the distribution of trend properties increased towards higher magnitudes, stronger TDIs, and lower TSSs (Fig 3), highlighting the potential influence of external factors on regional sea level trends. The Atlantic Ocean and Tropics exhibit the most significant shifts between the 1993-2000 and 2000-2021 periods (Fig 3). In the Atlantic Ocean, the trend magnitude increased from 2.5 mm/yr (1993-2000) to 3.5 mm/yr (2000-2021), accompanied by TDI of 98-99%. Despite the TSS:0.26% over the initial eight-year period indicating a small potential trend reversal, the TSS dropped to a mere 0.16% over the subsequent 21-year period (2000-2021), signifying a persistent stable trend. The shift in magnitude and TSS is observed for all six regions, and TDI changed slightly in the Atlantic, Pacific and Southern oceans. The TSS values across the six hotspots ranging from 0.00 to 1.17 indicate a low probability that the trends in these oceans could reverse over a 29-year period. In other words, the current trends in these oceans exceed the magnitude and plausibility of interannual to 29-year decadal oscillations, suggesting significant contributions from external forcing (e.g., ocean warming and land-ocean mass transport) as a driver. However, multi-decadal variability may still substantially contribute to RMSL rise in these regions. Internal variability influences short-term RMSL rise by accelerating during positive phases and decelerating during negative phases, ultimately resulting in less plausible (lower TDI), more uncertain, and less stable (higher TSS) trends over longer timescales.

# Discussion

In this study, we used satellite altimetry data over 29-year period (1993 – 2021) to evaluate trend dynamics in GMSL and RMSL using Gaussian process regression along with two probabilistic indices (TDI and TSS), in addition to trend magnitude. Our non-parametric Bayesian regression model incorporates kernels with distributions over functions, effectively smoothing the underlying latent trend processes and minimize the assumptions of traditional parametric methods (i.e., specificity, normality, homoscedasticity, and independency) [9]. By adhering to the sum rule, we quantified the probability of trend change and the persistent progression of the trend. Inclusion of indices beyond trend magnitude enables detection of trend dynamics (e.g., slight changes and overall robustness) and confines the rationale to available data; thereby eliminating the necessity for extended timescales to detect changes in trends. These new indices offer valuable insights into studying trend dynamics at smaller timescales and quantifying the impact of interannual processes (e.g., ENSO) or sporadic events in modulating trends, in addition to evaluating overall plausibility and stability.

For the GMSL, we analyzed the trend properties (magnitude, plausibility, and stability) and shifts in their distributions over the 29-year altimetry record. Our findings are consistent with those of previous studies, supporting the notion of GMSL acceleration during the altimetry record[2], as well as persistent acceleration since the 1960s[3] and those based on climate models[4]. Importantly, our approach provides a reliable estimate of acceleration by defining it as a positive shift in the trend properties distribution rather than using a single parametric value of quadratic fits. The persistent upward trend of the GMSL emphasizes the impact of external forcing, such as GHG emissions over natural climate variability. However, the interactions between multidecadal oscillations and feedback mechanisms between the warming trend and these oscillations cannot be entirely dismissed and warrant further investigation.

Our findings regarding La Niña-driven pauses in the GMSL are consistent with other studies that have argued that nonlinear trend fluctuations in the GMSL are comparable to ENSO fluctuations[28,29]. This study also demonstrates the diverse impacts of La Niña events or weak neutral anomalies, such as the 2013 event, and the approximately symmetric response of El Niño in modulating the GMSL trend (Fig 1). For RMSL, we identified six regions where the distribution of trend properties shifted from 1993 to 2021, displaying higher magnitudes, increased TDI, and lower TSS (Fig. 3). These findings are consistent with climate model ensemble estimates of persistent trends in the Pacific, Atlantic, Southern, and the Indian ocean[30]. Notably, we demonstrated that their average basin exhibits acceleration patterns and identified the North Sea as one of these regions (Fig. 3).

The Pacific Ocean experiences the smallest shift in magnitude distribution with an average increase from 2.5 mm/yr (1993-2000) to 3.1 mm/yr (2000-2021), accompanied with TDI (64-67%. However, the increased stability of the trend with TSS is evident, with a 9% probability of inverting over 2000 – 2021 compared with 86% over 1993-200. This observation over the entire Pacific Ocean suggests a persistent driving process, such as external forcing, which exceeds ENSO and PDO variability (Figs S4,12). Notably, the PDO exhibited four fluctuation cycles throughout the 29-year period (Fig. S3). Pacific trend variability, as shown by Hamlington, et al. [31], includes interannual and decadal contributions of ±1 mm/yr to the linear trend from the tropical western sections to the northeastern coast of the US. In the Atlantic Ocean, a rising sea-level trend is clear with magnitudes increasing from 2.5 mm/yr (1993-2000) to 3.5 mm/yr (2000-2021) (Fig 3). The AMO and external forcing likely contribute to this persistent trend. The phase of AMO has been positive since 1995 (Fig S4) with significant decadal periodicity (Fig S12). Local sea-level rise along the eastern coast of North America is associated with a weakening of the Atlantic Meridional Overturning Circulation[32], leading to increased tidal flooding[33]. Some studies argue that using up to a 60-year data record is inconclusive of an acceleration in sea-level rise due to 60-year oscillations in the AMO[34]

The results for the North Sea are consistent with the historical tide gauge data[35,36]. Changes in the Indian Ocean trend are less pronounced than those in the Atlantic and Southern oceans but show a relative increase (Fig. 3). The dominant natural variability in the Indian Ocean is the Dipole Mode Index, with decadal variability in the southwest linked to ENSO[37]. These oscillations are less likely to reproduce all the patterns of the rise which support other studies that have identified consistent patterns extending beyond natural variations[30,38].

The Southern Ocean displays a consistent trend, with the magnitude increasing from 2.9 mm/yr (1993-2000) to 3.2 mm/yr (2000-2021) (Fig 3), and the significant  periodicity Southern Ocean oscillations are predominately interannual (Fig S12). The persistence of the trend magnitude, plausibility, and stability suggest external forcing drivers, such as ocean warming, rather than interannual and decadal oscillations. These results  support Shi, et al. [39] who concluded that a significant acceleration of zonal flow in the Southern Ocean primarily results from anthropogenic ocean warming. The observed heterogeneity in regional trends stems from spatiotemporal variations in ocean warming and gravitational effects due to melting freshwater ice sheets and land water reservoirs, which fluctuate at multi-decadal scales[40].

One benefit of employing the methodology of this study is its ability to detect subtle shifts in trends across a multivariate context, enhancing trend attributions, which are crucial for sea-level rise trends. Moreover, this approach can refine empirical projections or reconstructions of sea levels by considering short-term trend dynamics and incorporating prior information.

Ultimately, adopting probabilistic reasoning can help researchers communicate their findings more effectively by quantifying sea-level trends and uncertainties using probabilities rather than plain assertions. This, in turn, allows policymakers and the public to better understand the uncertainties and implications of sea-level rise, fostering more informed discussions and decision-making processes.

## Materials and Methods

We used a non-parametric and interpretable Bayesian  model (i.e., Gaussian process regression) [41] to model GMSL and RMSL and derive their trend properties over 29 years from 1993 to 2021 based on

satellite altimetry data[42]. Here, we provide a brief description of the data and methods; more information is provided in the supplementary material (SM).

## Satellite Altimetry

We used the long-term mean of global and regional sea levels from satellites that have monitored the same ground tracks since 1992 (e.g., TOPEX/Poseidon, Jason-1, Jason-2, and Jason-3) and most of the altimeters of ERS-2, GFO, and Envisat. The data include estimates of the means for global oceans and 21 regional oceans, seas, and gulfs (Table S1). We used the ICE6G-D model[43] to derive and correct the contributions of the glacial isostatic adjustment (GIA) to sea surface height using the basin average. Data were then resampled into monthly periods, deseasonalized using harmonic regression, and regressed using Gaussian process regression to derive the trends, changes in trends, and their properties. We also used gridded altimetry data[44] to show variability in sea-level trends. These data were corrected also for GIA[43].

## Climate variability indices

The rates of increase in GMSL and RMSL are influenced by natural oceanic variability. Accurate attribution of trends in GMSL and RMSL necessitates data extending beyond the timescales of natural oceanic variabilities[8]. The extent to which these variabilities affect trends remains uncertain. Over the study period, we assessed the TDI of sea-level trends in relation to interannual to multidecadal climate variability by analyzing 12 key climate indices from 1960 through 2019. We examined the relationships between these indices and the observed sea-level trends, These indices include the Atlantic Meridional Mode (AMM), Atlantic Multidecadal Oscillation (AMO), Pacific Decadal Oscillation (PDO), Inter-decadal Pacific Oscillation (IPO), Arctic Oscillation (AO), Pacific North America (PNA), North Atlantic Oscillation (NAO), Tropical Northern Atlantic Index (TNAI), Tropical Southern Atlantic Index (TSAI), Southern Oscillation Index (SOI), El Niño Southern Oscillation (ENSO) Region 3.4 (Nino-3.4), and the Dipole Mode Index (DMI).

## Gaussian process regression (GPR)

We used a latent-Gaussian process model to regress the GMSLs and RMSLs and assess their dynamics. We assume that the trend driving processes ($f$) are random and continuous and gradually change over discrete times. The observable features for $f$ rise with hyperparameters ($\Theta$) and noise according to an additive model is (eq. 1).

$$Y_i = f(t_i) + \in_i \quad (1)$$

where $\in_i$ is independent noise with zero mean.

The trend is defined as the instantaneous slope df as the first derivative of $f$. Therefore, by sampling $f$ over discrete times, we can uncover dynamic properties of the trend:

$$df(t)\frac{df(s)}{ds}(t) \quad (2)$$

The probability of a positive trend conditioned on data, when $\delta < 0$

$$TDI(t, \delta|\Theta) = P(df(t + \delta) > 0|Y, t, \Theta) =$$

$$\frac{1}{2} + \frac{1}{2}Erf\left(\frac{\mu_{df}(t + \delta|\Theta)}{2^{1/2}\Sigma_{df}(t + \delta, t + \delta|\Theta)^{1/2}}\right) \quad (3)$$

where TDI is the trend direction index, a unitless probabilistic index between 0 and 1,
$\delta$ is the instantaneous slope at time t,
$\Theta$ is the hyperparameter of the GP kernel, and
Y is the vector of the input data.
The TSS can be estimated as:

$$TSS(t, \mathcal{T}|\Theta) = \lambda(t|\Theta)\varphi\left(\frac{\mu_{df}(t|\Theta)}{\Sigma_{df}(t, t|\Theta)^{1/2}}\right) \quad (4)$$

We invoke this rationale using GPR in the Bayesian domain over the time series of GMSL and RMSLs. We selected the radial basis function (RBF), which can capture the intercept and linear and quadratic features of the trend better than the other kernels[27].

We used Stan probabilistic programming[45] in the r framework[46] to perform the computations. We followed the following scenarios for the analysis: First, for a single time series, we ran eight independent Markov chains for 50,000 iterations using Hamilton Monte Carlo (HMC), where half of the samples used warm-p and destabilized the distributions, and the rest were used to sample the posterior distribution. The diagnostic models were constructed by generating a trace plot (Fig. S3) and investigating the $\hat{R}$ [47]. $\hat{R}$ conveys the convergence diagnostic of the chains by comparing the within and between estimates of the parameters and other modeling quantities of interest. Chains are mixed well when $\hat{R}$ is > 1. We evaluated the regression model and trend indices over 1000 points over the period of the time series and summarized the results using the $95^{th}$, $68^{th}$, and $50^{th}$ quantiles.

### Continuous wavelets transform.

We utilized the continuous wavelet transform (CWT)[48,49] to examine the periodicity and scales of natural climate variability. The CWT serves as an effective tool for analyzing non-stationary signals, such as the 12 climate index time series, by offering a representation of both the time and frequency domains. This approach enables identification of the dominant oscillatory modes and their temporal evolution.

### Data availability

This study used public data. Altimetry data can be accessed through (NOAA / NESDIS / STAR - Laboratory for Satellite Altimetry (LSA)). Monthly data of the climate variability indices can be accessed from (Climate Indices: Monthly Atmospheric and Ocean Time Series: NOAA Physical Sciences Laboratory). Access to gridded altimetry data is provided through (MEaSUREs Gridded Sea Surface Height Anomalies Version 2205 | PO.DAAC (nasa.gov)).
Replicated results are archived in (https://doi.org/10.18738/T8/IIU9ZA)

# References

1       Cazenave, A. *et al.* The rate of sea-level rise. *Nature Climate Change* **4**, 358-361 (2014). https://doi.org:10.1038/nclimate2159

2       Nerem, R. S. *et al.* Climate-change-driven accelerated sea-level rise detected in the altimeter era. *Proc Natl Acad Sci U S A* **115**, 2022-2025 (2018). https://doi.org:10.1073/pnas.1717312115

3       Dangendorf, S. *et al.* Persistent acceleration in global sea-level rise since the 1960s. *Nature Climate Change* **9**, 705-710 (2019).

4       Stocker, T. F. *Climate change 2013: the physical science basis: Working Group I contribution to the Fifth assessment report of the Intergovernmental Panel on Climate Change.* (Cambridge University Press, 2014).

5       Cazenave, A. & Llovel, W. Contemporary sea level rise. *Ann Rev Mar Sci* **2**, 145-173 (2010). https://doi.org:10.1146/annurev-marine-120308-081105

6       İz, H. B. & Shum, C. The certitude of a global sea level acceleration during the satellite altimeter era. *Journal of Geodetic Science* **10**, 29-40 (2020).

7       Ablain, M. *et al.* Improved sea level record over the satellite altimetry era (1993–2010) from the Climate Change Initiative project. *Ocean Sci* **11**, 67-82 (2015).

8       Hamlington, B. D., Frederikse, T., Nerem, R. S., Fasullo, J. T. & Adhikari, S. Investigating the acceleration of regional sea level rise during the satellite altimeter era. *Geophys Res Lett* **47**, e2019GL086528 (2020).

9       Scott, M. & Chandler, R. *Statistical methods for trend detection and analysis in the environmental sciences.* (John Wiley & Sons, 2011).

10      Ocana, V., Zorita, E. & Heimbach, P. Stochastic secular trends in sea level rise. *Journal of Geophysical Research: Oceans* **121**, 2183-2202 (2016).

11      Zhang, X. & Church, J. A. Sea level trends, interannual and decadal variability in the Pacific Ocean. *Geophys Res Lett* **39** (2012).

12      Hoeke, R. K. *et al.* Widespread inundation of Pacific islands triggered by distant-source wind-waves. *Global Planet Change* **108**, 128-138 (2013).

13      Penduff, T., Llovel, W., Close, S., Garcia-Gomez, I. & Leroux, S. Trends of coastal sea level between 1993 and 2015: Imprints of atmospheric forcing and oceanic chaos. *Surv Geophys* **40**, 1543-1562 (2019).

14      Zhu, Y. *Studies of the Long-term Change of Global Mean and Regional Sea Surface Height*, University of South Florida, (2019).

15      Visser, H., Dangendorf, S. & Petersen, A. C. A review of trend models applied to sea level data with reference to the "acceleration-deceleration debate". *Journal of Geophysical Research: Oceans* **120**, 3873-3895 (2015).

16      Boretti, A. Is there any support in the long term tide gauge data to the claims that parts of Sydney will be swamped by rising sea levels? *Coast Eng* **64**, 161-167 (2012).

17      Houston, J. R. & Dean, R. G. Effects of sea-level decadal variability on acceleration and trend difference. *J Coastal Res* **29**, 1062-1072 (2013).

18      Hunter, J. R. & Brown, M. Discussion of Boretti, A.,'Is there any support in the long term tide gauge data to the claims that parts of Sydney will be swamped by rising sea levels?', Coastal Engineering, 64, 161–167, June 2012. *Coast Eng* **75**, 1-3 (2013).

19      Watson, P. J. A new perspective on global mean sea level (GMSL) acceleration. *Geophys Res Lett* **43**, 6478-6484 (2016).

20      Jaynes, E. T. *Probability theory: The logic of science.* (Cambridge university press, 2003).

21      Johnson, D. H. The insignificance of statistical significance testing. *The journal of wildlife management*, 763-772 (1999).

22      Kim, S.-J., Koh, K., Boyd, S. & Gorinevsky, D. \ell_1 trend filtering. *Siam Rev* **51**, 339-360 (2009).

23      Oelsmann, J. *et al.* Bayesian modelling of piecewise trends and discontinuities to improve the estimation of coastal vertical land motion: DiscoTimeS: a method to detect change points in GNSS, satellite altimetry, tide gauge and other geophysical time series. *J Geodesy* **96**, 62 (2022).

24      Zhao, K. *et al.* Detecting change-point, trend, and seasonality in satellite time series data to track abrupt changes and nonlinear dynamics: A Bayesian ensemble algorithm. *Remote Sens Environ* **232**, 111181 (2019).

25      Tadesse, M. G. *et al.* Long-term trends in storm surge climate derived from an ensemble of global surge reconstructions. *Scientific Reports* **12**, 13307 (2022).

26      Gottlieb, A. & Müller, H.-G. A stickiness coefficient for longitudinal data. *Computational Statistics & Data Analysis* **56**, 4000-4010 (2012).

27      Jensen, A. K. & Ekstrøm, C. T. Quantifying the trendiness of trends. *Journal of the Royal Statistical Society Series C* **70**, 98-121 (2021).

28      Boening, C., Willis, J. K., Landerer, F. W., Nerem, R. S. & Fasullo, J. The 2011 La Niña: So strong, the oceans fell. *Geophys Res Lett* **39**, n/a-n/a (2012). https://doi.org:10.1029/2012gl053055

29      Piecuch, C. G. & Quinn, K. J. El Niño, La Niña, and the global sea level budget. *Ocean Sci* **12**, 1165-1177 (2016). https://doi.org:10.5194/os-12-1165-2016

30      Fasullo, J. T. & Nerem, R. S. Altimeter-era emergence of the patterns of forced sea-level rise in climate models and implications for the future. *Proceedings of the National Academy of Sciences* **115**, 12944-12949 (2018).

31      Hamlington, B. D. *et al.* Past, Present, and Future Pacific Sea-Level Change. *Earth's Future* **9**, e2020EF001839 (2021).

32      Sallenger Jr, A. H., Doran, K. S. & Howd, P. A. Hotspot of accelerated sea-level rise on the Atlantic coast of North America. *Nature Climate Change* **2**, 884-888 (2012).

33      Ezer, T. & Atkinson, L. P. Accelerated flooding along the US East Coast: On the impact of sea-level rise, tides, storms, the Gulf Stream, and the North Atlantic Oscillations. *Earth's Future* **2**, 362-382 (2014).

34      Parker, A. Oscillations of sea level rise along the Atlantic coast of North America north of Cape Hatteras. *Nat Hazards* **65**, 991-997 (2013).

35      Sallenger, A. H., Doran, K. S. & Howd, P. A. Hotspot of accelerated sea-level rise on the Atlantic coast of North America. *Nature Climate Change* **2**, 884-888 (2012).

36      Steffelbauer, D. B., Riva, R. E., Timmermans, J. S., Kwakkel, J. H. & Bakker, M. Evidence of regional sea-level rise acceleration for the north sea. *Environmental Research Letters* (2022).

37      Han, W. *et al.* Indian Ocean Decadal Variability: A Review. *B Am Meteorol Soc* **95**, 1679-1703 (2014). https://doi.org:10.1175/bams-d-13-00028.1

38      Han, W. *et al.* Patterns of Indian Ocean sea-level change in a warming climate. *Nat Geosci* **3**, 546-550 (2010).

39      Shi, J.-R., Talley, L. D., Xie, S.-P., Peng, Q. & Liu, W. Ocean warming and accelerating Southern Ocean zonal flow. *Nature Climate Change* **11**, 1090-1097 (2021).

40      Nicholls, R. J. & Cazenave, A. Sea-level rise and its impact on coastal zones. *Science* **328**, 1517-1520 (2010).

41      Rasmussen, C. E. & Williams, C. K.    (MIT Press, 2006).

42      Chelton, D. B., Ries, J. C., Haines, B. J., Fu, L.-L. & Callahan, P. S. in *International geophysics* Vol. 69 1-ii (Elsevier, 2001).

43      Peltier, R., Argus, D. F. & Drummond, R. Comment on "An assessment of the ICE-6G_C (VM5a) glacial isostatic adjustment model" by Purcell et al. *Journal of Geophysical Research: Solid Earth* **123**, 2019-2028 (2018).

44      Fournier, S., Willis, J. K., Killett, E., Qu, Z. & Zlotnicki, V. JPL MEaSUREs Gridded Sea Surface Height Anomalies Version 2205.

45      Gelman, A., Lee, D. & Guo, J. Stan: A probabilistic programming language for Bayesian inference and optimization. *Journal of Educational and Behavioral Statistics* **40**, 530-543 (2015).

46      Team, R. C. *R: A language and environment for statisticaln computing. R Foundation for Statistical Computing, Vienna, Austria*, <https://www.R-project.org/> (2021).

47      Vehtari, A., Gelman, A., Simpson, D., Carpenter, B. & Bürkner, P.-C. Rank-normalization, folding, and localization: an improved R for assessing convergence of MCMC (with discussion). *Bayesian analysis* **16**, 667-718 (2021).

48      Grossmann, A. & Morlet, J. Decomposition of Hardy functions into square integrable wavelets of constant shape. *SIAM journal on mathematical analysis* **15**, 723-736 (1984).

49      Torrence, C. & Compo, G.    (Co, 1998).

Figures
**Fig 1.** Global mean sea level trend analysis. [a] GMSL time series using the GPR model, with uncertainties. [b] Trend slope magnitude evolution from 1993 to 2021. [c] Trend Detection Index (TDI) indicating the upward GMSL trend probability. La Niña events in the Pacific Ocean correspond to short trend pauses. [e] Trend shift score reflecting slope changes and potential slope direction shifts.

**Table 1.** Summary of GMSL trend properties: Annual characteristics of global sea level rise, including trend magnitude, plausibility degree, and shift score from 1993 to 2021, based on altimetry data.

**Fig 2.** Regional sea level trends: Mean TDI for 20 regional seas and oceans during 1993-2021, based on altimetry data.

**Fig 3.** Posterior density of global mean and regional sea level trend magnitudes. Posterior density for GMSL and six RMSL regions with three high posterior interval levels between 1993 and 2021. Vertical lines show mean trend magnitudes for three periods (1993-2000; 2000-2021; and 1993–2021), with accompanying plausibility (average TDI) and stability (average TSS). TSS over a certain period represents the probability of an opposite (i.e., downward) trend change. Global maps show the linear trend of sea level between 1993 and 2021.
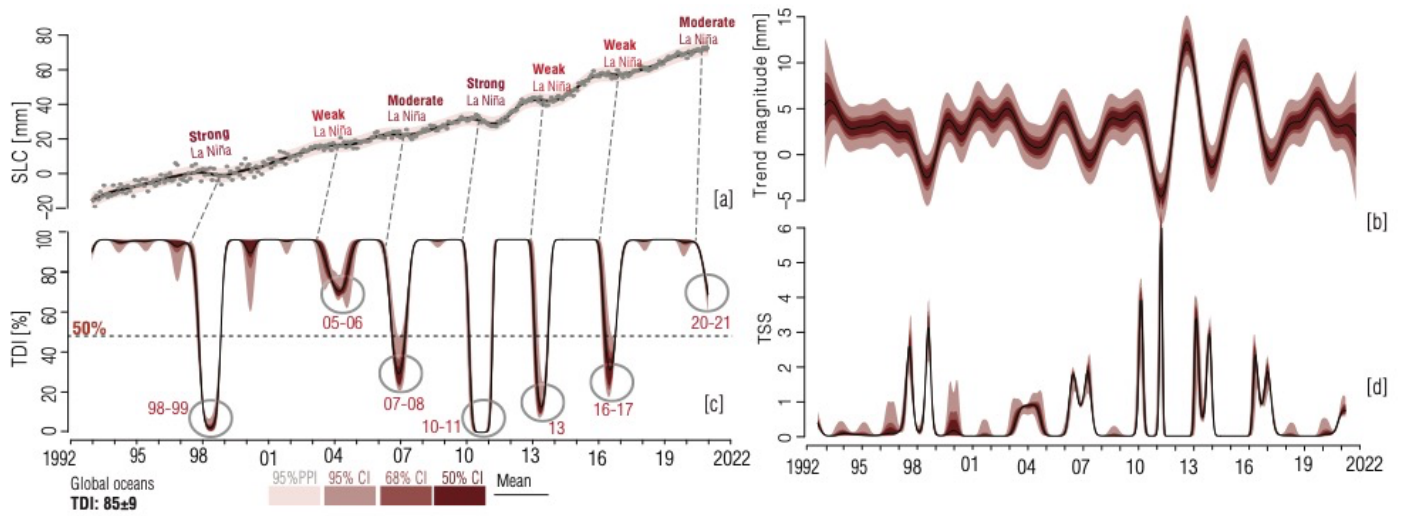
**Fig 1.** Global mean sea level trend analysis. [a] GMSL time series using the GPR model, with uncertainties. [b] Trend slope magnitude evolution from 1993 to 2021. [c] Trend Detection Index (TDI) indicating the upward GMSL trend probability. La Niña events in the Pacific Ocean correspond to short trend pauses. [e] Trend stability score reflecting slope changes and potential slope direction shifts

Table 1. Summary of GMSL trend properties: Annual characteristics of global sea level rise, including trend magnitude, plausibility degree, and stability score from 1993 to 2021, based on altimetry data.

| Year | Trend magnitude (mm/yr) | | | Trend Plausibility (TDI) % | | | Trend Stability (TSS) | | |
|------|------|------|-------|------|------|-------|------|------|-------|
| | Mean | 2.5% | 97.5% | Mean | 2.5% | 97.5% | Mean | 2.5% | 97.5% |
| 1993 | 5.13 | 1.20 | 9.14 | 99% | 98% | 100% | 0.08 | 0.04 | 0.18 |
| 1994 | 2.98 | 0.50 | 5.44 | 99% | 96% | 100% | 0.07 | 0.00 | 0.26 |
| 1995 | 3.22 | 0.80 | 5.63 | 99% | 97% | 100% | 0.05 | 0.00 | 0.24 |
| 1996 | 3.00 | 0.47 | 5.44 | 98% | 92% | 100% | 0.09 | 0.00 | 0.46 |
| 1997 | 1.49 | -0.94 | 4.16 | 80% | 71% | 87% | 0.89 | 0.49 | 1.39 |
| 1998 | -1.53 | -4.28 | 0.90 | 17% | 14% | 23% | 1.00 | 0.70 | 1.30 |
| 1999 | 3.04 | 0.57 | 5.78 | 98% | 95% | 99% | 0.23 | 0.14 | 0.45 |
| 2000 | 3.24 | 0.54 | 5.79 | 97% | 85% | 100% | 0.16 | 0.00 | 0.75 |
| 2001 | 4.31 | 1.73 | 6.87 | 100% | 97% | 100% | 0.02 | 0.00 | 0.19 |
| 2002 | 4.55 | 2.13 | 7.10 | 100% | 99% | 100% | 0.01 | 0.00 | 0.06 |
| 2003 | 1.98 | -0.50 | 4.37 | 90% | 82% | 95% | 0.44 | 0.24 | 0.81 |
| 2004 | 1.19 | -1.27 | 3.60 | 81% | 71% | 91% | 0.69 | 0.38 | 1.06 |
| 2005 | 4.03 | 1.65 | 6.52 | 100% | 99% | 100% | 0.03 | 0.00 | 0.12 |
| 2006 | 0.94 | -1.53 | 3.33 | 68% | 61% | 80% | 0.88 | 0.62 | 1.12 |
| 2007 | 1.48 | -0.98 | 3.99 | 76% | 68% | 83% | 0.78 | 0.57 | 1.04 |
| 2008 | 3.88 | 1.31 | 6.34 | 100% | 98% | 100% | 0.02 | 0.00 | 0.15 |
| 2009 | 4.03 | 1.56 | 6.61 | 99% | 98% | 100% | 0.09 | 0.03 | 0.34 |
| 2010 | -2.56 | -5.21 | 0.03 | 16% | 8% | 23% | 0.91 | 0.38 | 1.47 |
| 2011 | 5.08 | 2.49 | 7.69 | 79% | 75% | 87% | 0.98 | 0.38 | 1.69 |
| 2012 | 8.23 | 5.68 | 10.81 | 99% | 97% | 100% | 0.17 | 0.00 | 0.45 |
| 2013 | -0.14 | -2.71 | 2.37 | 45% | 33% | 65% | 1.63 | 0.88 | 2.38 |
| 2014 | 7.08 | 4.64 | 9.52 | 100% | 100% | 100% | 0.01 | 0.01 | 0.02 |
| 2015 | 7.75 | 5.27 | 10.20 | 100% | 100% | 100% | 0.01 | 0.00 | 0.06 |
| 2016 | 0.51 | -2.29 | 2.69 | 57% | 43% | 73% | 1.33 | 0.77 | 1.80 |
| 2017 | 2.89 | 0.47 | 5.48 | 97% | 95% | 98% | 0.22 | 0.17 | 0.36 |
| 2018 | 4.85 | 2.28 | 7.34 | 100% | 98% | 100% | 0.02 | 0.00 | 0.14 |
| 2019. | 4.71 | 1.94 | 7.03 | 100% | 97% | 100% | 0.03 | 0.00 | 0.20 |
| 2020 | 3.20 | -0.79 | 6.84 | 93% | 90% | 95% | 0.32 | 0.22 | 0.52 |
| 2021 | 2.55 | -5.07 | 9.16 | 72% | 62% | 77% | 0.70 | 0.51 | 1.01 |

**Fig 2.** Regional sea level trends: Mean TDI for 21 regional seas and oceans during 1993-2021, based on altimetry data.
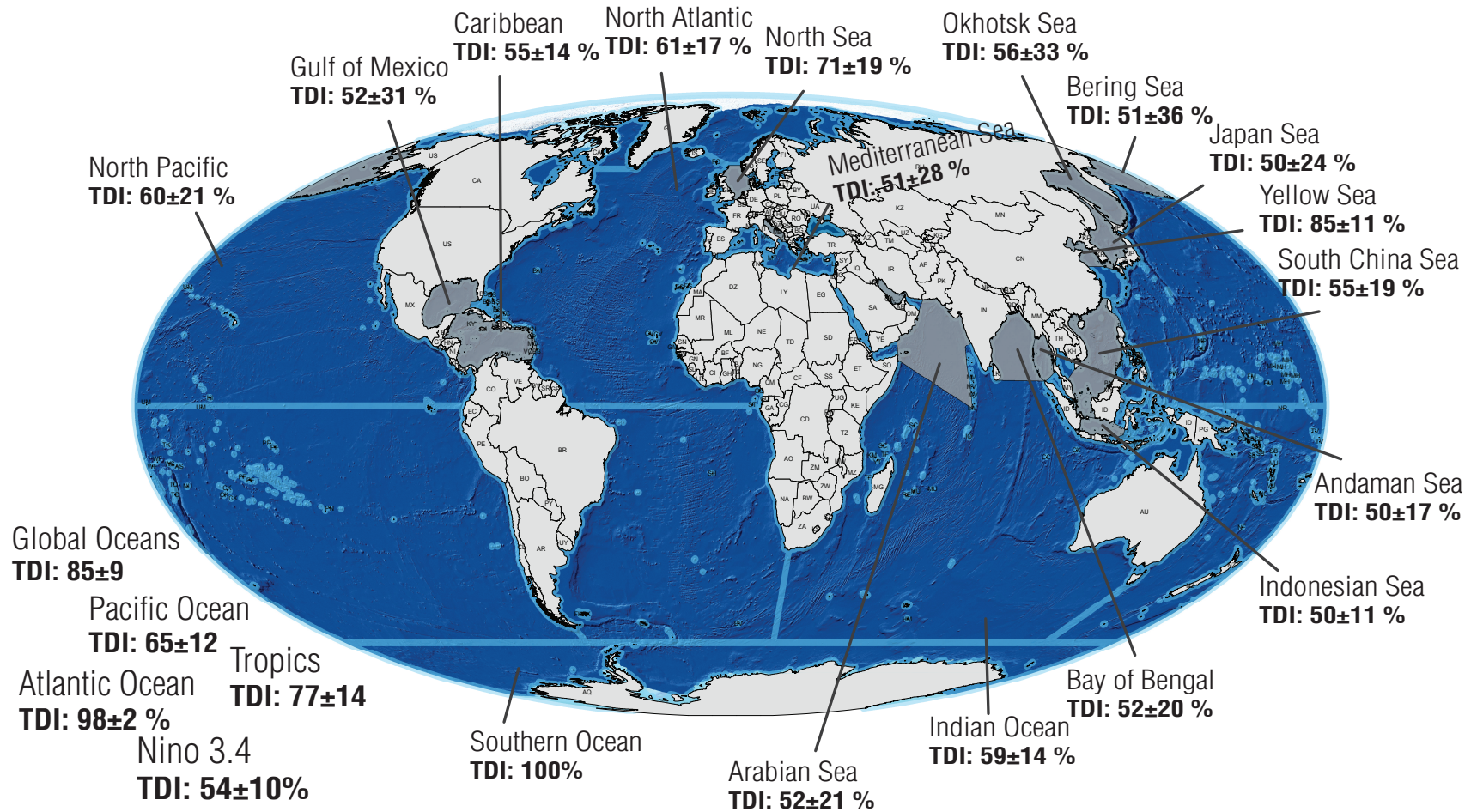
**Fig 3.** Posterior ... posterior interval levels between 1993 and 2021. Vertical lines show mean trend magnitudes for three periods (1993-2000; 2000-2021; and 1993–2021), with accompanying trend strength (TDI) and trend stability (TSS) indices. TSS over a certain period represents the probability of an opposite (i.e., downward) trend change. Global map show the linear trend of sea level between 1993 and 2021.

Supplementary materials
For

***Demystifying the Dynamics of Global and Regional Sea Level Trends from 1993 to 2021***

Ashraf Rateb[1]; Bridget R. Scanlon[1]

[1]Bureau of Economic Geology, University of Texas at Austin, Austin 78758, Texas United States

1 section
12 figures

## Gaussian Process Regression (GPR)

GPR overcomes the limitations of traditional modeling (e.g., linear and quadratic) by relaxing their limited assumptions over the process ($f$) (e.g., linearity). GPR assumes that $f$ is a random process generated from a multivariate Gaussian distribution, and can be smoothed by tuning their infinite parameters, defined as a kernel.

$$\begin{bmatrix} f(x_i) \\ f(x_j) \\ f(x_k) \\ \vdots \end{bmatrix} \sim \mathcal{N} \left( \begin{bmatrix} m(x_i) \\ m(x_j) \\ m(x_k) \\ \vdots \end{bmatrix}, \begin{bmatrix} k(x_i, x_i) & k(x_i, x_j) & k(x_i, x_k) & \cdots \\ k(x_j, x_i) & k(x_j, x_j) & k(x_j, x_k) & \cdots \\ k(x_k, x_i) & k(x_k, x_j) & k(x_k, x_k) & \cdots \\ \vdots & \vdots & \vdots & \ddots \end{bmatrix} \right) \tag{7}$$

Where the $x$ is the observed process,
(i, j, k) are time indices,
$m, k$ and are the mean and covariance functions, respectively.
The random function ($f$) can be inferred using the Bayesian theorem and its posterior is a Gaussian distribution. The assumption of *smoothness* or closeness can be encoded by using a covariance function $k$. Various types of functions can be modeled, including linear and nonlinear functions, by modifying the different mean and covariance functions of the distributions. This flexibility allows us to account for the different complexities of the underlying process. The GPR is robust to overfitting.
The posterior over functions follow Bayes' theorem, as follows:

$$p(\mathbf{f}|X, y) \propto p(y|\mathbf{f})p(\mathbf{f}|X) \tag{8}$$

where $y$ is the likelihood based on observations, and $p(\mathbf{f}|X)$ represents the priors that follow the GP distribution as:

$$p(\mathbf{f}|X) \sim \mathcal{N}(\mathbf{f}|\boldsymbol{\mu}(X), \mathbf{K}((X, X)) \tag{9}$$

where $\mathbf{f}$ vector for all function values over the time index
$\boldsymbol{\mu}(X)$ is a vector for all mean functions, and
$\mathbf{K}((X, X)$ is the covariance matrix between the inputs.

The covariance functions (also known as the kernel) are our initial reasoning for the functions that we want to model. Many kernels can be regressed (e.g., linear, periodic, white noise, rational quadratic, polynomial, and radial basis functions). Here, we choose to regress the CVT using the square exponential, which has been proven to capture the intercept, linear, and quadratic features of underlying process [1]. RBF is defined as:

$$K_{RBF}(x, \dot{x}) = \sigma^2 exp\left(-\frac{(x-\dot{x})^2}{2\lambda^2}\right) \tag{10}$$

Where $\sigma$ is the variance noise
$\lambda$ is the length scale of the function (horizontal change of the function); the larger the value of $\lambda$, the higher the smoothness of the functions, and vice versa **(Fig. S2)**.
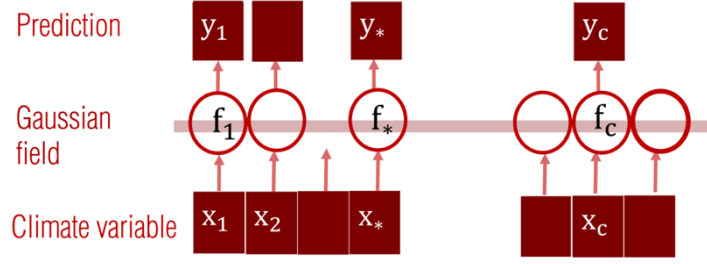
**Fig. S1.** Graphical representation of the Gaussian process.

[a]

[b]
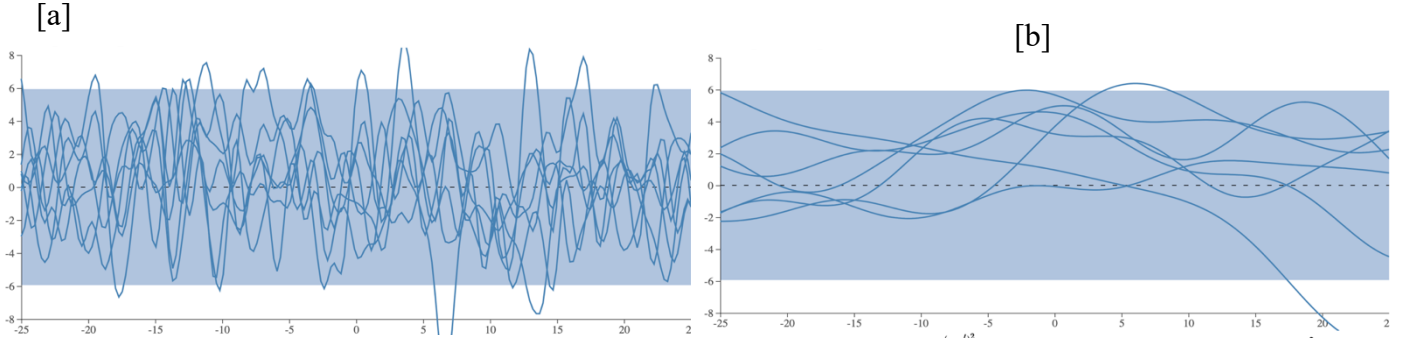


**Fig. S2.** Length scale parameter $\lambda$ in RBF kernel. [a] RBF with $\lambda = 0.7$, [b] RBF with $\lambda=4$.

The RBF kernels assume that our desired functions are smooth and infinitely differentiable, which holds for the CVT. For rapid changes in f, the RBF can be replaced by the rational quadratic kernel, which does not assume smoothness but includes a power parameter in addition to the RBF parameters. The power parameter controls the speed of the local variations. RQ can be seen as generalization of RBF with different lengths scale functions. Both Kernels RBF and RQ and tested over the CVT, and the results showed the RQ is capturing the short-term variations (e.g., 2-3 year) fluctuations in the time series besides the long term.

## Trendiness indices

Two probabilistic indices were proposed to assess the trendiness of random process [1]: the Trend Direction Index (TDI) and the trend shift score (TSS).

**Trend Direction Index (TDI)**

The TDI quantifies the probability of the random process $(f)$ trend is changing monotonicity at the observed time (x) conditioned on the data. At any given time, the instantaneous slope df(t) increases when (df(t) >0) or decreases when (df(t)<0) which can be deduced from the probability distribution of $f$. TDI herein is the probability of the change in df(t) sign. The TDI estimates provide plausible answers to these questions. What is the probability (e.g., climate trend) of progressing or de-progressing?

TDI can be estimated from the posterior distribute of df as

$$TDI(t, \delta|\Theta) = P(df(t + \delta) > 0|Y, t, \Theta) =$$

$$\frac{1}{2} + \frac{1}{2} Erf \left( \frac{\mu_{df}(t + \delta|\Theta)}{2^{1/2} \Sigma_{df}(t + \delta, t + \delta|\Theta)^{1/2}} \right) \quad (12)$$

where $\delta$ is the instantaneous slope at time t, $\Theta$ is the hyperparameter of the RBF kernel, Y is the vector of the input data. The dominator represents the posterior mean and covariance. $TDI(t, \delta|\Theta)$ is trending in the upward direction, where $\mu_{df}(t + \delta|\Theta) \neq 0$ indicates that the posterior mean of df is not constant and progressive in the upward or downward directions as follows:

3

$$TDI(t, \delta|\Theta) = \begin{cases} Unknown, & \mu_{df}(t + \delta|\Theta) = 0 \\ Trending_{up}, & \mu_{df}(t + \delta|\Theta) \neq 0 \end{cases} \qquad (13)$$

$$TDI(t, \delta|\Theta)_{down} = 1 - TDI(t, \delta|\Theta)_{up} \qquad (14)$$

TDI over time interval t indicates the local probability of trending the underlying process (e.g., sea level) conditioned on the observed data at t. The TDI over the whole conditioned data reveals the average numeric global plausibility of the process trend. Different thresholds can be provided for TDI to consider *plausible* applications. For complete derivatives of TDI and TSS, the reader is referred to[1]

**Trend Shift Score (TSS)**

TSS is the number of observed monotonic changes in the trend at time, conditioned on the observed data. A trend is called *stable* if the df does not change sign (i.e., does not cross zero). A small TSS indicates a smaller number of changes in the trend; thus, it is a stable trend (e.g., GSLR tends), and vice versa for unstable trends (e.g., ENSO index). TSS also can be regarded as the higher bound probability of observing at least one sign change of the trend [1]

The local TSS at any given time is given by

$$dTSS(t, \mathcal{T}|\Theta) = \lambda(t|\Theta)\varphi\left(\frac{\mu_{df}(t|\Theta)}{\Sigma_{df}(t, t|\Theta)^{1/2}}\right) \qquad (15)$$

The global TSS over the entire conditioned data is the integration of the local dTSS as

$$TSS(\mathcal{I}|\Theta) = \int dTSSI\ (t|\Theta)dt \qquad (16)$$

**Estimand and Estimator**

We consider the Bayesian estimator instead of the maximum likelihood to infer the hype-parameters $\Theta$ estimators for a consistent computation and to propagate the uncertainty of these parameters through posterior distributions.

Our data generation process is governed by a hierarchal model, as

$$f|\beta, \theta \sim \mathcal{GP}(\mu_\beta(.), C_\theta(., .)). \qquad (17)$$
$$Y_i|t_i f(t_i), \Theta \sim \mathcal{N}(f(t_i), \sigma^2), \qquad \Theta = (\beta, \theta, \sigma)$$

$\beta$ is a vector parameter of the mean functions
$\theta$ is vector of parameter of the covariance functions
$\sigma$ is the standard deviation of the CVT.

For the priori

$$(\beta, \theta, \sigma) \sim \mathcal{G}(\mathbf{\Theta}|\psi, t) \qquad (18)$$

where G is a family of distributions (i.e., student), indexed by $\psi$.

Factorization of the model distributions is

$$P(Y, f(t), \mathbf{\Theta}|\psi, t) = P(Y|f(t), \mathbf{\Theta}|\psi, t), P(f(t)|\mathbf{\Theta}|\psi, t)\mathcal{G}(\mathbf{\Theta}|\psi, t) \qquad (19)$$

The posterior distribution is

$$P(\mathbf{\Theta}|Y, \psi, t) = \frac{\mathcal{G}(\mathbf{\Theta}|\psi, t)P(Y|\mathbf{\Theta}, \psi, t)}{P(Y|\psi, t)} =$$
$$\frac{\mathcal{G}(\mathbf{\Theta}|\psi, t) \int P(Y|f(t), \mathbf{\Theta}, \psi, t)dP(f(t)|\mathbf{\Theta}, \psi, t)}{\iint P(Y|f(t), \mathbf{\Theta}, \psi, t)\ dP(f(t)|\mathbf{\Theta}, \psi, t)d\mathcal{G}(|\mathbf{\Theta}, \psi, t))}$$
$$(20)$$

We summarized the results of the distributions over TDI and TSS using their mean and 95, 66%, and 50% credible intervals.

Following [1], we used standard probabilistic programming [2] in framework [3] to carry out the computations. Two scenarios were followed, First, for the CVT, (i.e., GSL regions, and ice loss in ice sheets, glaciers basins, and aquifer TW), we obtained a single time series for each location, and ran eight independent Markov chain for $50 \times 10^3$ iterations using Hamilton Monet Carlo, (here in MCMC) where the half were used to warm-p and destabilize the distributions, and the rest used to sample the posterior distributions. Model diagnostics were performed by generating trace plots ( Fig. S3), and examining $\hat{R}$ [4]. $\hat{R}$ conveys the convergence diagnostic of the MCMC chains by comparing the within and between estimates for the parameters and other modeling quantities of interests. The chains were mixed well when $\hat{R}$Is > 1. We evaluated the regressed models and indices over 1000 points over the time frame of the time series (29-year) and the results were summarized using different quantiles.
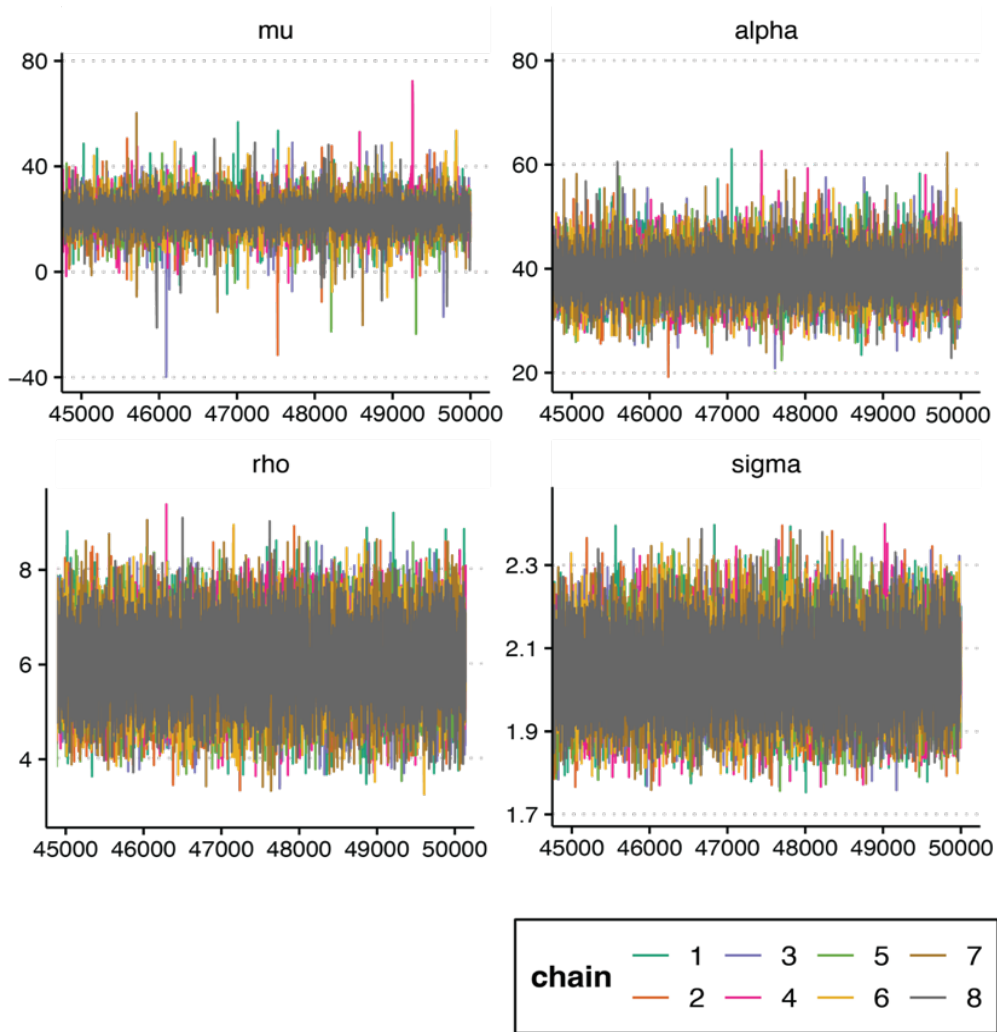


**Fig. S3.** MCMC diagnostic plot. An example MCMC trace plots the GSL time series using eight Markov chains to generate 50,000 samples for the GPR hyperparameters. Only last 5000 samples are shown for figure clarity.

,
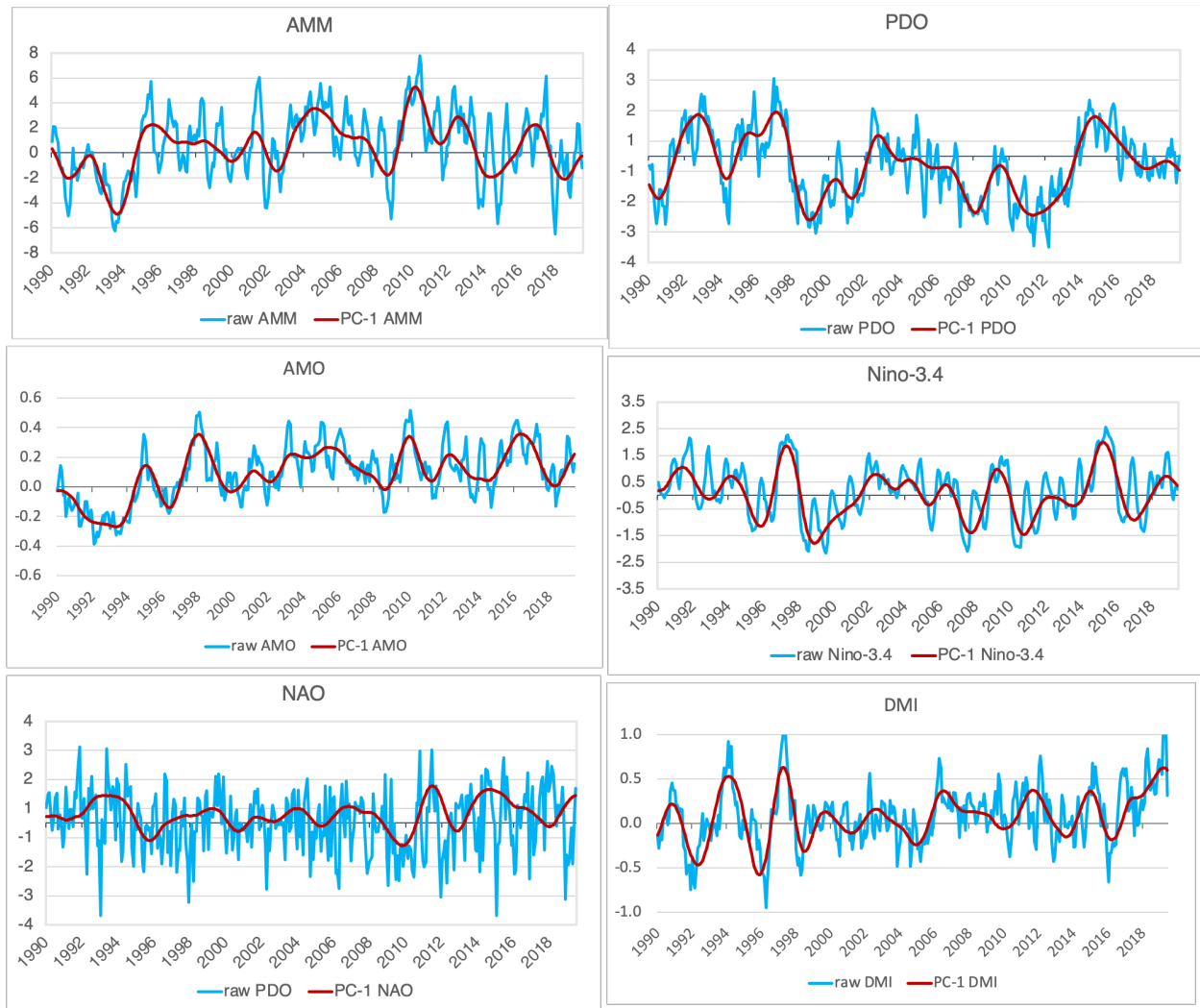
**Fig S4**. Indices of Climate Variability: Time series depicting common modes of interannual and decadal variability in the Pacific (PDO), Atlantic (AMM, AMO, NAO), and Indian (DMI) Oceans. Light blue is the raw time series, and red is the firs
t principal component [5]
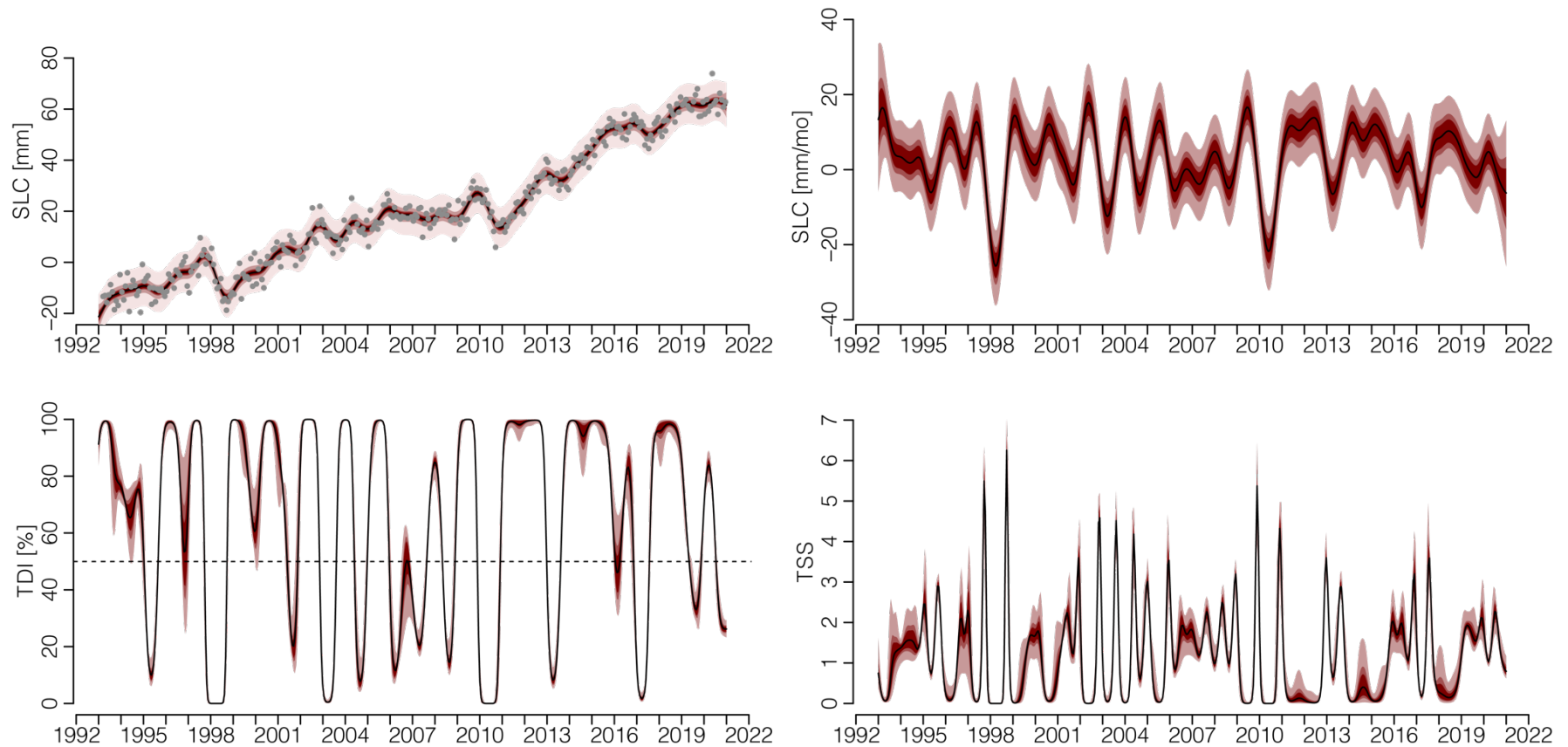
**Fig. S5**. GPR and Trendiness of the Pacific Ocean. In the first row (left), observations from altimetry data and GPR using the RBF kernel with three credible intervals (CIs) are presented. The second row (left) indicates the TDI (in the upward direction), and the dashed horizontal line where TDI = 50% represents unknown trendiness. The TDI in the downward direction is equivalent to 100 - TDI. On the second row (right), the TSS is displayed, indicating the periods of trend stability.
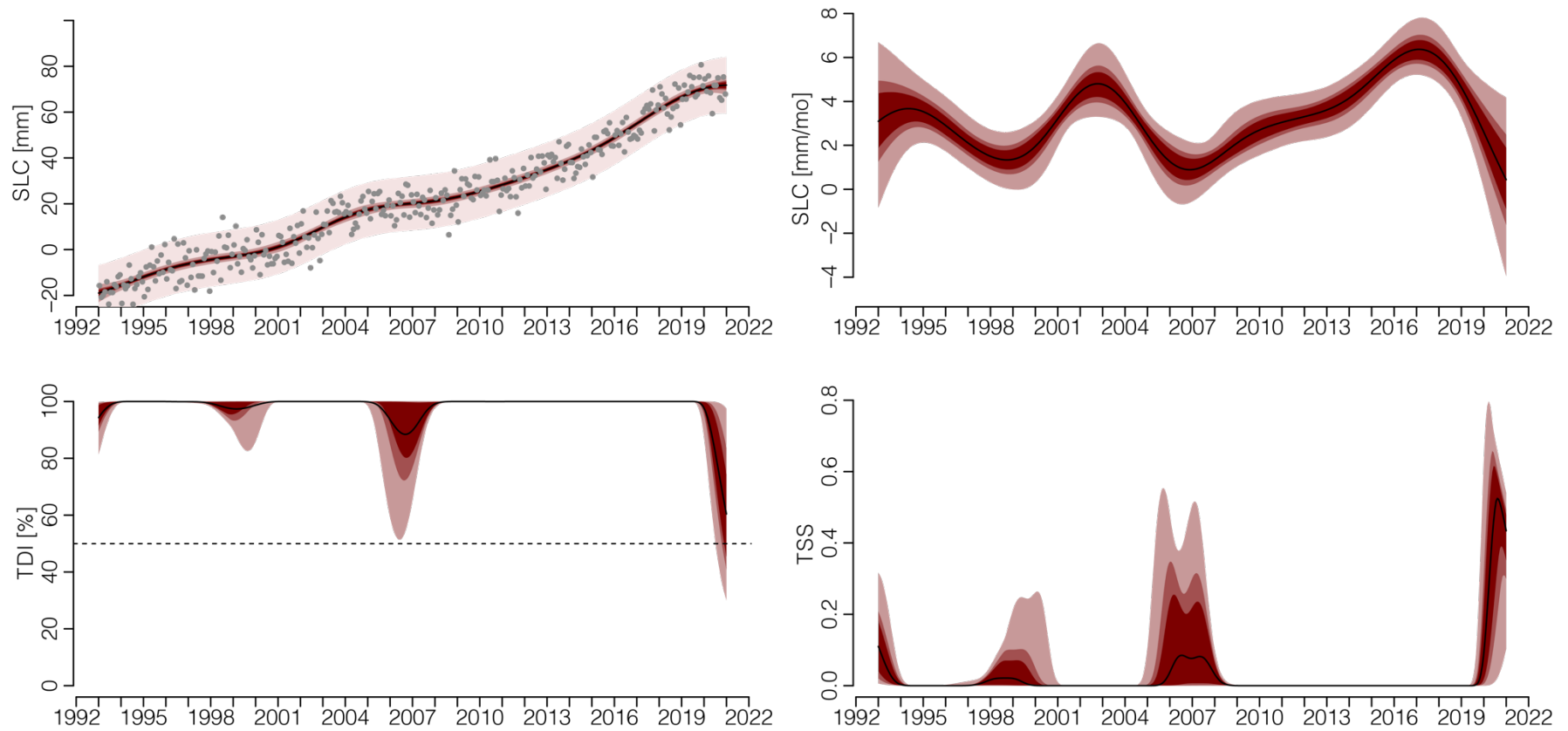
**Fig. S6**. GPR and Trendiness of the Atlantic Ocean. On the first row (left), observations from altimetry data and GPR using an RBF kernel with three credible intervals (CIs) are shown. The second row (left) indicates the TDI (in the upward direction), and the dashed horizontal line where TDI = 50% represents unknown trendiness. The TDI in the downward direction is equivalent to 100 - TDI. On the second row (right), the TSS is displayed, indicating the periods of trend stability.
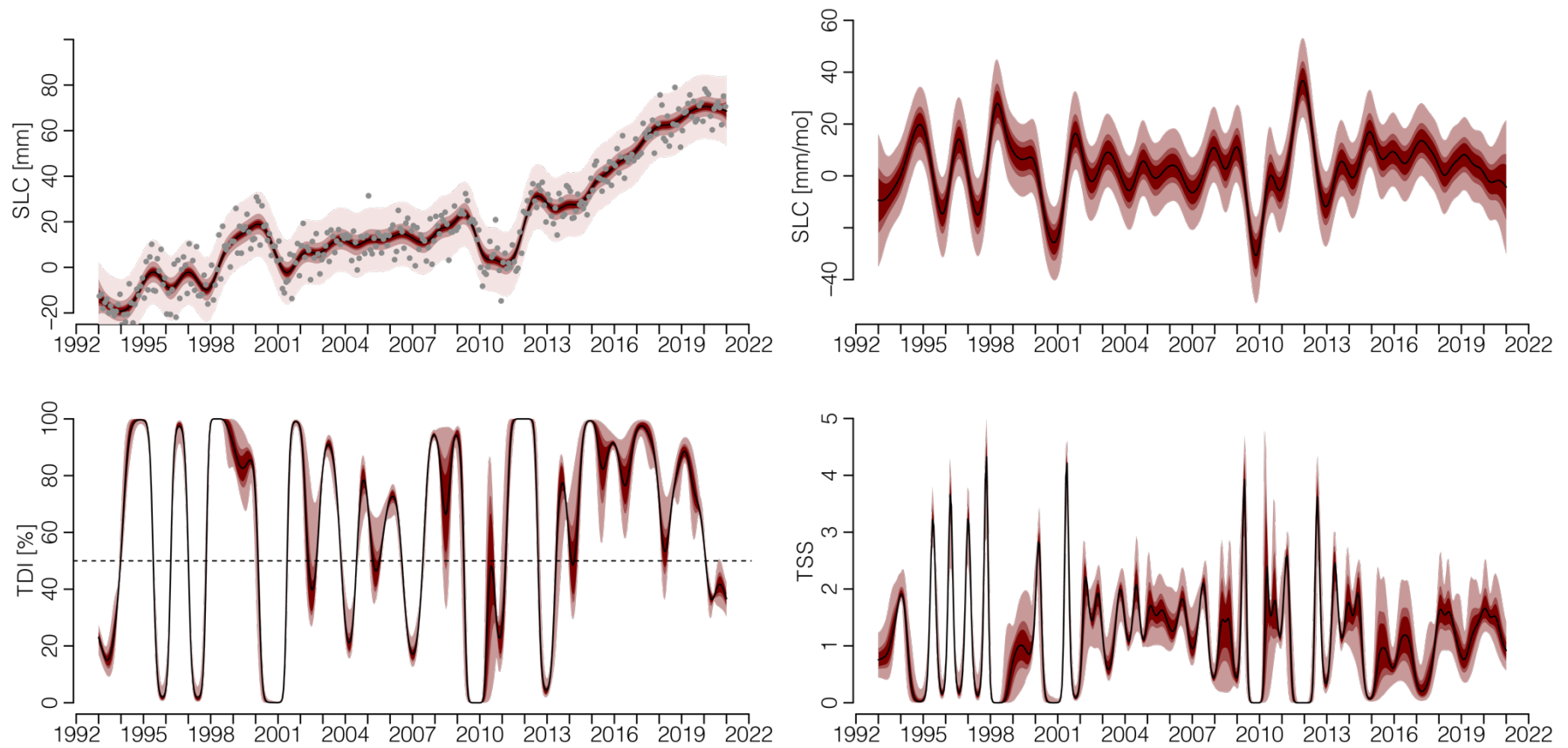
**Fig. S7.** GPR and Trendiness of the North Atlantic Ocean. On the first row (left), observations from altimetry data and GPR using an RBF kernel with three credible intervals (CIs) are shown. The second row (left) indicates the TDI (in the upward direction), and the dashed horizontal line where TDI = 50% represents unknown trendiness. The TDI in the downward direction is equivalent to 100 - TDI. On the second row (right), the TSS is displayed, indicating the periods of trend stability.
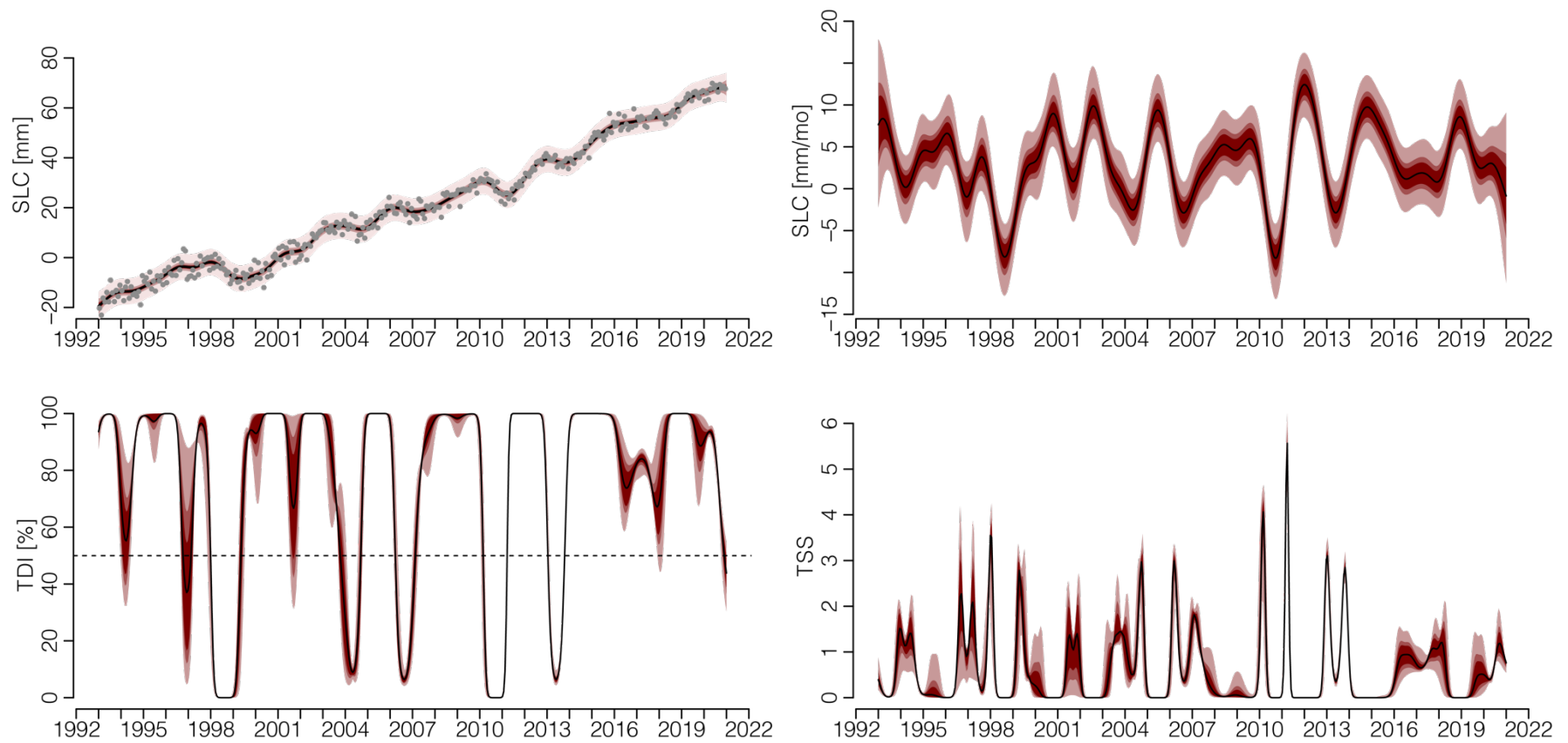
**Fig. S8**. GPR and Trendiness of the topical regions of the oceans. On the first row (left), observations from altimetry data and GPR using an RBF kernel with three credible intervals (CIs) are shown. The second row (left) indicates the TDI (in the upward direction), and the dashed horizontal line where TDI = 50% represents unknown trendiness. The TDI in the downward direction is equivalent to 100 - TDI. On the second row (right), the TSS is displayed, indicating the periods of trend stability.
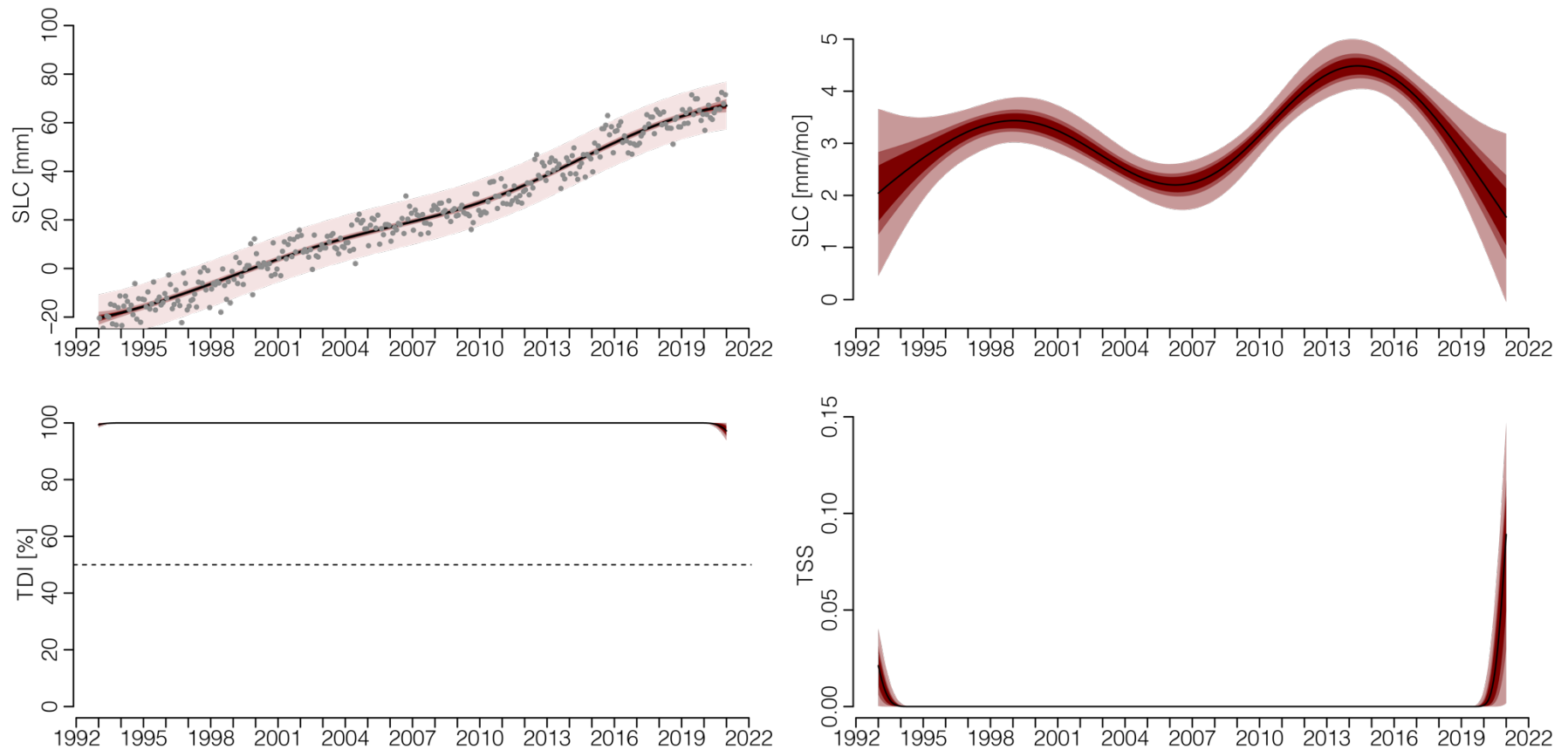
**Fig. S9**. GPR and Trendiness of the Southern ocean. On the first row (left), observations from altimetry data and GPR using an RBF kernel with three credible intervals (CIs) are shown. The second row (left) indicates the TDI (in the upward direction), and the dashed horizontal line where TDI = 50% represents unknown trendiness. The TDI in the downward direction is equivalent to 100 - TDI. On the second row (right), the TSS is displayed, indicating the periods of trend stability.
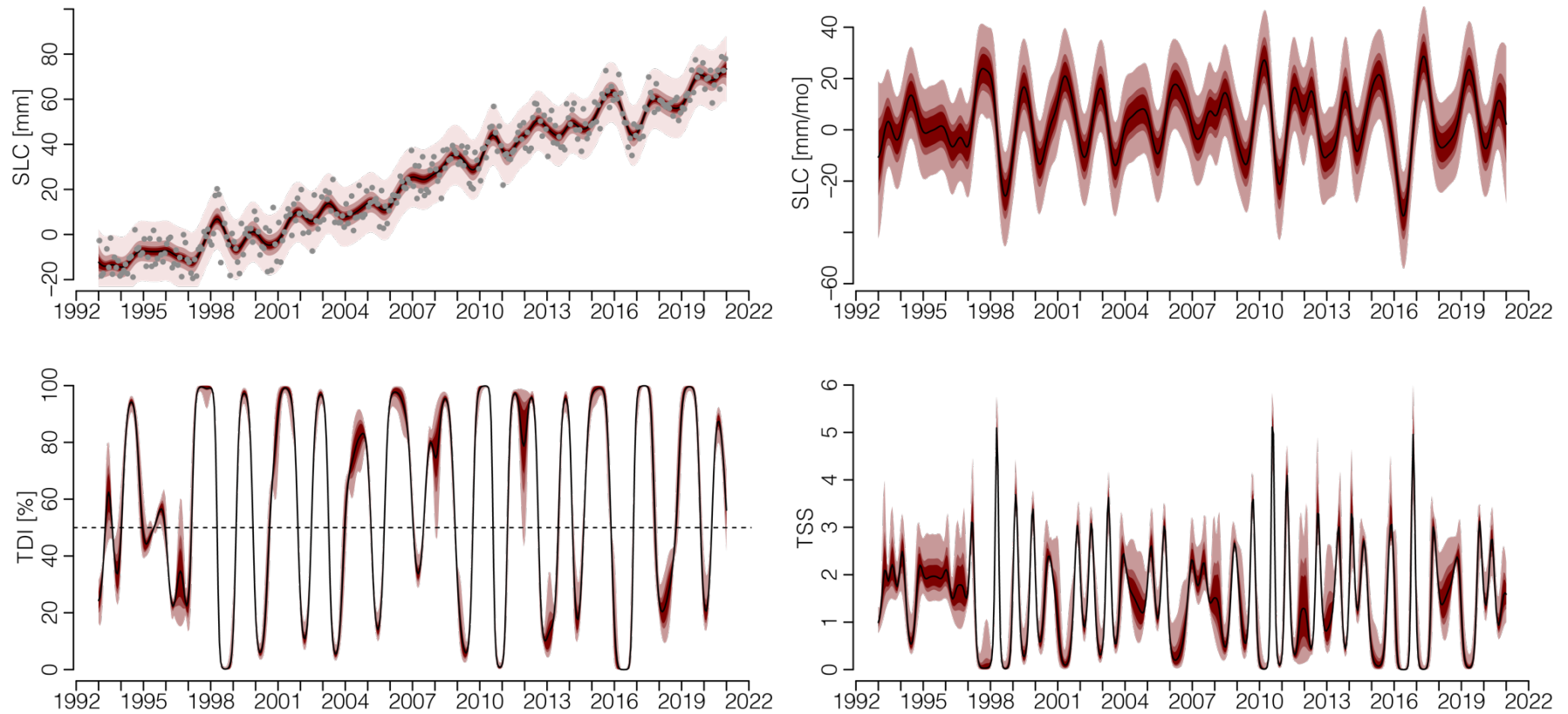
**Fig. S10.** GPR and Trendiness of the Indian ocean. On the first row (left), observations from altimetry data and GPR using an RBF kernel with three credible intervals (CIs) are shown. The second row (left) indicates the TDI (in the upward direction), and the dashed horizontal line where TDI = 50% represents unknown trendiness. The TDI in the downward direction is equivalent to 100 - TDI. On the second row (right), the TSS is displayed, indicating the periods of trend stability.
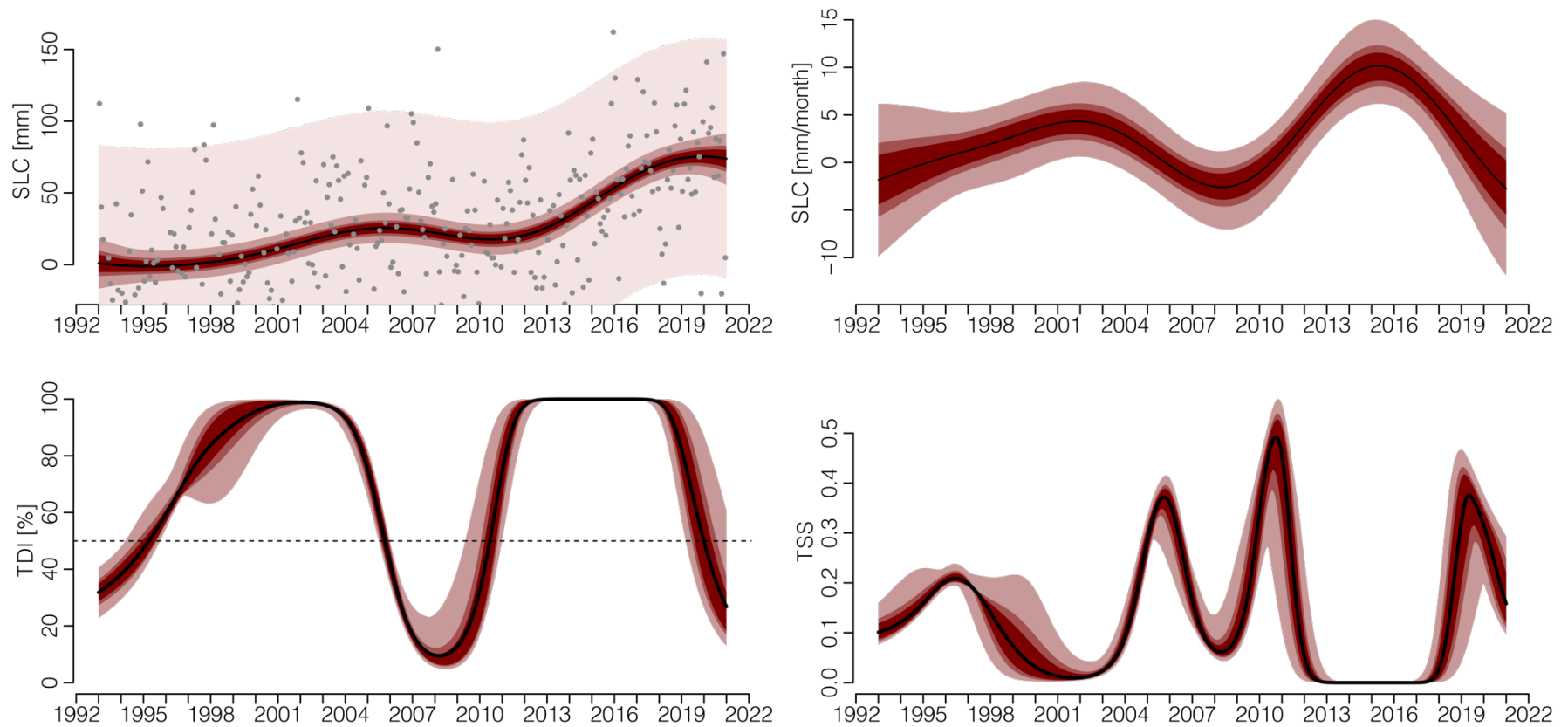
**Fig. S11.** GPR and Trendiness of the North sea. On the first row (left), observations from altimetry data and GPR using an RBF kernel with three credible intervals (CIs) are shown. The second row (left) indicates the TDI (in the upward direction), and the dashed horizontal line where TDI = 50% represents unknown trendiness. The TDI in the downward direction is equivalent to 100 - TDI. On the second row (right), the TSS is displayed, indicating the periods of trend stability.
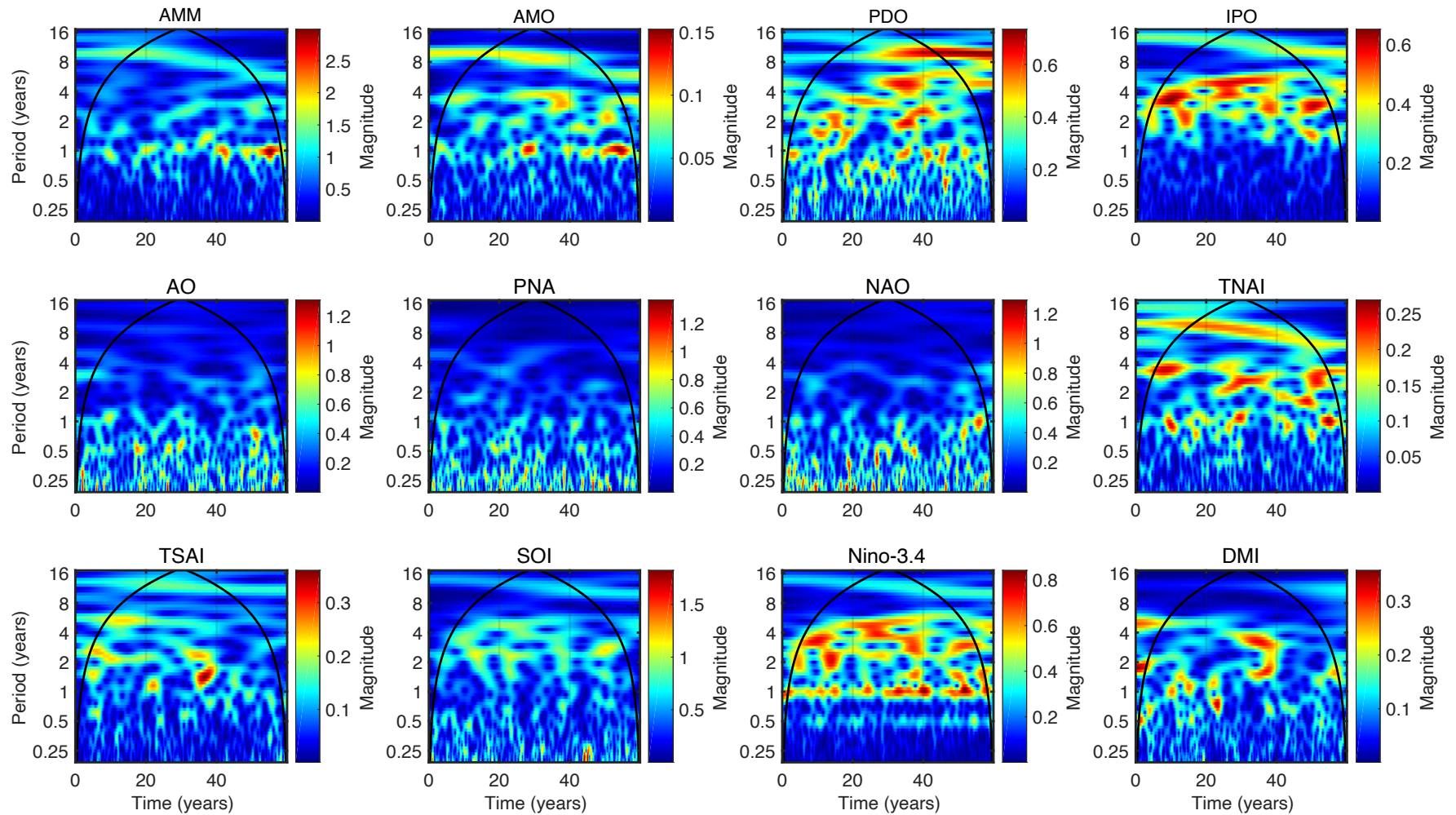
**Fig. S12**. Continuous Wavelet Transform of Periodicity Scales (**1960-2019):** This figure illustrates the analysis of 12 climate variability indices in the Pacific, Atlantic, Indian, Arctic, and Southern Oceans using continuous wavelet transform techniques. Indices include AMM (Atlantic Meridional Mode), AMO (Atlantic Multidecadal Oscillation), PDO (Pacific Decadal Oscillation), IPO (Interdecadal Pacific Oscillation), AO (Arctic Oscillation), PNA (Pacific North America pattern), NAO (North Atlantic Oscillation), TNAI (Tropical Northern Atlantic Index), TSAI (Tropical Southern Atlantic Index), SOI (Southern Oscillation Index), Nino-3.4 (El Niño Southern Oscillation Region 3.4), and DMI (Dipole Mode Index).

Other supplementary materials
**Excel file:**
SI_data_repoducible_figures_02_01_2023.xlsx
10 Tables

## References

1       Jensen, A. K. & Ekstrøm, C. T. Quantifying the trendiness of trends. *Journal of the Royal Statistical Society Series C* **70**, 98-121 (2021).

2       Gelman, A., Lee, D. & Guo, J. Stan: A probabilistic programming language for Bayesian inference and optimization. *Journal of Educational and Behavioral Statistics* **40**, 530-543 (2015).

3       Team, R. C. *R: A language and environment for statisticaln computing. R Foundation for Statistical Computing, Vienna, Austria*, <https://www.R-project.org/> (2021).

4       Vehtari, A., Gelman, A., Simpson, D., Carpenter, B. & Bürkner, P.-C. Rank-Normalization, Folding, and Localization: An Improved $\widehat{R}$ for Assessing Convergence of MCMC (with Discussion). *Bayesian Analysis* **16**, 667-718, 652 (2021).

5       Kim, K.-Y., Hamlington, B. & Na, H. Theoretical foundation of cyclostationary EOF analysis for geophysical and climatic variables: concepts and examples. *Earth-science reviews* **150**, 201-218 (2015).